An Experimental Investigation of the Effects of Aeroelastic Couplings on Aeromechanical Stability of a Hingeless Rotor Helicopter

William G. Bousman
Research Scientist
Aeromechanics Laboratory
U.S. Army Research & Technology Laboratories (AVRADCOM)
Moffett Field, California 94035

PRESENTED AT THE 36TH ANNUAL FORUM
OF THE
AMERICAN HELICOPTER SOCIETY
WASHINGTON, D.C.
MAY 1980

PREPRINT NO. 80-25

An Experimental Investigation of the Effects of Aeroelastic Couplings on Aeromechanical Stability of a Hingeless Rotor Helicopter

William G. Bousman
Research Scientist
Aeromechanics Laboratory
U.S. Army Research & Technology Laboratories (AVRADCOM)
Moffett Field, California 94035

Abstract

A 1.62-m diameter rotor model was used to investigate aeromechanical stability, and the results were compared to theory. Configurations tested included: (1) a non-matched stiffness rotor as a baseline, (2) the baseline rotor with negative pitch-lag coupling, (3) the combination of negative pitch-lag coupling and structural flap-lag coupling on the baseline rotor, (4) a matched stiffness rotor, and (5) a matched stiffness rotor with negative pitch-lag coupling. The measured lead-lag regressing mode damping of the five configurations agreed well with theory, but only the matched stiffness case with negative pitch-lag coupling was able to stabilize the air resonance mode. Comparison of theory and experiment for the damping of the body modes showed significant differences that may be related to rotor inflow dynamics.

Introduction

The problem of aeromechanical instability of a helicopter in hover, commonly referred to as air or ground resonance, is a complex phenomenon involving both the rotor and body degrees of freedom in which the rotor lead-lag regressing mode may become unstable. The use of a simplified analytical model, as described in Reference 1, is of considerable value in obtaining an understanding of the aeromechanical instability phenomena and the means by which it may be eliminated. The work reported in that reference suggested ways in which aeroelastic coupling of various rotor degrees of freedom could be used to stabilize the lead-lag regressing mode and obviate the need for rotor lead-lag dampers. For the case of a conventional or non-matched stiffness rotor where the flapping stiffness is less than the lead-lag stiffness, it was shown that the addition of negative pitch-lag coupling was stabilizing in hovering flight for rotor speeds where the lead-lag regressing mode coupled with the body roll mode, but destabilizing in the vicinity of the body pitch mode. If flap-lag structural coupling was combined with negative pitch-lag coupling, then the lead-lag regressing mode was stable over all rotor speeds. It was also demonstrated that for a matched stiffness configuration, the addition of negative pitch-lag coupling was stabilizing for the full range of rotor speeds. The results of Reference 1 were calculated for specific configurations, and therefore could not establish the general validity of the various couplings as means of avoiding instability. Nevertheless, the results did suggest promising design approaches.

An experimental program was undertaken with a relatively simple, small-scale model rotor and fuselage to examine helicopter aeromechanical instabilities in a manner analogous to the theoretical approach of Reference 1. Initial experiments investigated the problems involved in measurements of this nature, and obtained data for use in validating the theoretical model.[2] Unfortunately, differences between the theoretical and experimental models prevented a direct comparison of the results, and for correlation purposes, a more sophisticated analytical model was used[3] that had originally been developed for the analysis of bearingless rotors. The theory and experiment were first compared for the case of a rotor in simulated vacuum conditions, and then for a hingeless rotor of conventional stiffness under normal conditions. In the former case, the effects of a vacuum were approximated by using tantalum rods instead of blades. The resulting correlation was quite good and provided considerable confidence in the structural modeling used in the analysis. The correlation for the rotor with conventional stiffness was also good, but raised a number of questions about possible limitations of the aerodynamic model. It was felt that more data were required to observe the effects of blade pitch angle on aeromechanical stability and to assess the validity of the aerodynamic model. In addition, nonlinear damping in the gimbal ball bearings prevented adequate measurements of the body mode damping, and it was therefore not possible to judge the adequacy of the analytical model for these modes.

The present experiments were undertaken with two primary objectives. The first objective was to correct the problem with the gimbal bearings revealed in Reference 2 so that accurate measurements of body modal damping could be made; and, secondly, to extend the measurements to include configurations with pitch-lag coupling, flap-lag coupling, and matched flapping and lead-lag stiffnesses. The experiment, therefore, should provide

considerably more data for the validation of the theoretical model, and in addition allow a judgment of the adequacy of the techniques proposed in Reference 1 for stabilizing the lead-lag regressing mode.

The paper starts with a description of the rotor model that was tested. Changes to the model to correct the deficiencies identified in Reference 2 are emphasized, as well as the methods used to obtain the aeroelastic couplings and stiffness variation. Test procedures are discussed, as well as the way the modal behavior is identified, and each mode's frequency and damping are determined. A very brief discussion of the theoretical model of Reference 3 is given, and then the results of the experiment are presented.

Experimental Model

The model used in the experiment has a 1.62-m diameter, three-bladed rotor which is mounted on a static mast. The mast, in turn, is bolted to a transmission and two electric drive motors, which together constitute the body of the model. The model is supported in a gimbal frame which allows pitch and roll motions, and the gimbal frame is supported on a stand of considerable rigidity. An overall view of the model is shown in Figure 1. Descriptive properties of the model are contained in the Appendix.

Figure 1. Overall view of model.

The rotor was designed so that most of the blade flexibility is concentrated in root flexures. An expanded view of one of these root flexures is shown in Figure 2.

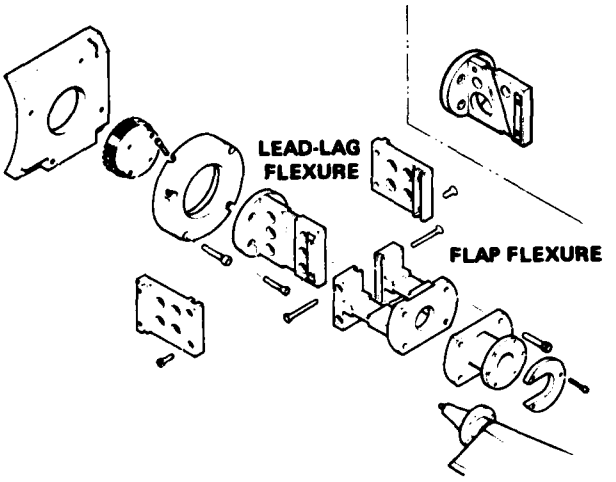

Figure 2. Expanded view of blade root flexures.

From the center of the hub, the lag hinge is first, and the flap hinge is outboard. The load path from the lag hinge to the flap hinge is folded back so that when assembled the flexure centerlines are coincident. All joints are bolted to reduce damping due to friction. The structural damping of the flexure and blade combination is approximately 0.5% critical damping. The low blade damping makes the experimental measurement problem easier, but is a lower level than would be expected with a full-scale rotor. The blade pitch angle is changed manually, and this may be done either outboard or inboard of the flexures. The lead-lag stiffness of the blade-root flexures illustrated in Figure 2 is considerably greater than the flap stiffness, and in this respect represents a conventional or nonmatched stiffness hingeless rotor design. To test the behavior of a matched stiffness rotor, a second set of flap flexures were made with an approximately eightfold increase in flap stiffness so that the nonrotating flap and lead-lag frequencies were equal with the blade set at zero pitch. For pitch angles greater than zero, there was some variation in the frequencies due to blade flexibility, and in this respect the flexures did not show ideal matched stiffness behavior. Negative pitch-lag coupling was incorporated in the rotor by substituting a skewed lag hinge for the straight lag hinge (see inset of Figure 2). The skewing of this flexure provides a pitch-lag coupling, θ_ζ, of -0.4. To combine structural flap-lag coupling, the blade pitch angle was set inboard of the flexures so that the principal axes of

the flexure and blade structure had the same orientation as the blade aerodynamic pitch angle, therefore coupling the flapping and lead-lag motions elastically.

The body modal damping was nonlinear with amplitude for the experiments reported in Reference 2 due to the ball bearings used in the gimbal frame. For this experiment the gimbal frame was redesigned to replace the ball bearings with flexural pivots. These pivots are very soft torsionally and have essentially no damping. The only body damping on the model, then, is due to various connections across the gimbal such as power cables and cooling water for the motors, oil lines, thermocouples, and instrumentation. The body roll damping was linear, while a slight nonlinearity was evident for body pitch. Measurements of body damping taken through the course of the experiment stayed within ±15% of the nominal values listed in the Appendix.

The body frequencies are controlled by cantilever springs mounted across the gimbal flexural pivots. One set of springs was used for the entire experiment. The body pitch spring was selected to provide a dimensionless body pitch frequency of about 0.12 at the nominal rotor speed of 720 rpm, and the roll spring was chosen to give a dimensionless roll frequency of about 0.28. As the rotor dimensionless lead-lag frequency is 0.70 for these conditions, this places the lead-lag regressing mode frequency at 0.30. Thus, the pitch mode is considerably lower in frequency than the lead-lag regressing mode, while the roll mode frequency is quite close and represents a critical design condition. This placement of the body frequencies corresponds with the values used in Reference 1, and is also representative of air resonance conditions for a number of full-scale soft inplane rotor helicopters.[4-7] The dimensional values of the body pitch and roll frequencies are, respectively, about 2 and 4 Hz. The gimbal frame and stand were designed to keep the higher-frequency elastic modes well above this range. The nearest elastic modes are mast pitching and rolling at about 45 Hz.

Two methods were used to excite the rotor and body modes in order to measure their frequency and damping from the transient decay. For the lead-lag regressing mode, a shaker was used to oscillate the model about its roll axis at the lead-lag regressing mode frequency. The shaker, which is mounted at the base of the stand as shown in Figure 1, is connected to the model with a pneumatic clamp that is actuated only during excitation. When excitation is stopped, the clamp opens, and the rotor and body motions are unrestrained. The body modes were excited by deflecting the model in either pitch or roll using a system of strings and pulleys. Having deflected the model, the string is quickly released, and the model motions are allowed to decay. Spurious damping can be introduced to the body motions if the operator does not manage a quick release. In the event of an instability, a snubbing mechanism located beneath the model can be used to lock out the body pitch and roll motions. This snubber is actuated manually under normal circumstances, but in the event of excessive loads in the lead-lag flexures, the snubber will automatically lock up the body.

Test Procedures and Analysis

The blade root flexures were instrumented with strain-gage bridges to measure the flap, lead-lag, and torsional deflections. The flapping and lead-lag signals for each blade were brought out through a set of slip rings, and were combined using a multiblade transform to generate flap sine and cosine coordinates, β_s and β_c; and lead-lag sine and cosine coordinates, ζ_s and ζ_c. The β_s and β_c coordinates represent the rotor-disk tilting: deflection in the β_s coordinate represents disk tilt side-to-side, while the β_c coordinate describes fore-and-aft tilting of the disk. The ζ_s and ζ_c coordinates represent side-to-side and fore-and-aft rotor center of gravity position in an analogous manner. The rotor progressing and regressing modes appear in the fixed system essentially as a wobbling of the disk either forward or backward with respect to the rotor direction. The lead-lag regressing mode, therefore, appears in both the ζ_s and ζ_c coordinates, the major difference being that the motions are 90° out of phase with each other. Except at very low rotor speeds, the regressing and progressing modes are well separated in frequency. The body pitch and roll flexural pivots were also instrumented with strain-gage bridges, and these provided a measure of the body pitch and roll deflections.

Rotor speed was used as the primary variable in the experiment. By varying rotor speed, the dimensionless lead-lag and flapping frequencies simulated designs from stiff to soft inplane. At each rotor speed, the lead-lag regressing mode was excited, and normally two transient records were obtained. For zero pitch-angle cases, the body pitch and roll modes were also excited. Fewer records were taken for pitch angles other than zero. Normally, the effect of pitch-angle variation was investigated at seven rotor speeds for the lead-lag regressing mode, and a single rotor speed for the body pitch and roll modes.

For each test condition, the transient data from the six coordinates, sine and cosine flapping, sine and cosine lead-lag, and body pitch and roll, were displayed on a CRT. Depending upon which mode had been excited, the coordinate was selected with the largest response, the data edited, if necessary, and the Fast Fourier Transform (FFT) of the signal obtained. The FFT was displayed on the CRT and the modal frequency identified. The moving-block analysis was then used to identify the modal damping. In addition, the amplitude and phase of the mode in each coordinate was calculated, assisting identification of the modal behavior.

Theoretical Model

The theoretical model used for comparison with the experimental results is described in Reference 3. Two modifications, one slight and the other more significant, have been made to this analysis since the correlation of Reference 2. The first modification allows the effects of airfoil camber to be included in the aerodynamic calculations and therefore provides a better representation of the experimental airfoil. The second modification is to extend the original analysis to handle the case of a hinge with spring restraint in lieu of a flexure element. This hinged or articulated representation makes correlation possible with the skewed lag hinge used in the experimental model to provide pitch-lag coupling.

Model properties required for the theoretical model are given in the Appendix. These properties are either derived from geometric data, such as the rotor radius and solidity, or determined by nonrotating measurements, as with the body and blade inertias. The flap and lead-lag stiffness values used in the analysis are calculated to match the blade nonrotating frequencies with the body degrees of freedom locked out.

Experimental Results and Comparison with Theory

Lead-Lag Regressing Mode Damping for Various Aeroelastic Couplings

Five rotor configurations were tested to examine the effects of the various couplings. These configurations are characterized by whether the nonrotating flap stiffness is much less than the lead-lag stiffness (nonmatched stiffness) or whether the stiffnesses are matched, whether the rotor includes negative pitch-lag coupling, and whether the flapping and lagging motions are structurally coupled. The properties of these five configurations are identified in Table 1. When the blade pitch angle is set inboard of the flexures, the principal axes of the blade and flexures rotate with the blade pitch angle, providing structural flap-lag coupling. As theory shows that structural flap-lag coupling is effective only when the flap and lead-lag stiffnesses are different, no attempt was made to test a configuration with matched stiffness and structural flap-lag coupling.

The behavior of the five configurations at a blade-pitch angle of 9° is compared in Figure 3. The lead-lag regressing mode damping is shown over a range of rotor speeds from approximately 500 to 1000 rpm, which represents soft inplane rotor designs with dimensionless lead-lag frequencies from 0.9 to 0.6. The rotor thrust will vary significantly over this range of rotor speeds for a constant blade pitch angle; however, these data can be considered an approximate equivalent of an air resonance condition. For Configuration 1, which represents the baseline case, as rotor speed is increased there is a slight reduction in the damping as the lead-lag regressing mode couples with the body pitch mode. Then, with a further increase in rotor speed, the rotor becomes unstable due to the coupling of the lead-lag regressing and

Table 1. Experimental Rotor Configurations

Configuration	Flap flexure	Lead-lag flexure	Blade pitch angle set
1	Nominal, $\omega_{\beta o} < \omega_{\zeta o}$	Straight, $\theta_\zeta = 0$	Outboard of flexures
2	Nominal, $\omega_{\beta o} < \omega_{\zeta o}$	Skewed, $\theta_\zeta = -0.4$	Outboard of flexures
3	Nominal, $\omega_{\beta o} < \omega_{\zeta o}$	Skewed, $\theta_\zeta = -0.4$	Inboard of flexures
4	Thick, $\omega_{\beta o} = \omega_{\zeta o}$	Straight, $\theta_\zeta = 0$	Outboard of flexures
5	Thick, $\omega_{\beta o} = \omega_{\zeta o}$	Skewed, $\theta_\zeta = -0.4$	Outboard of flexures

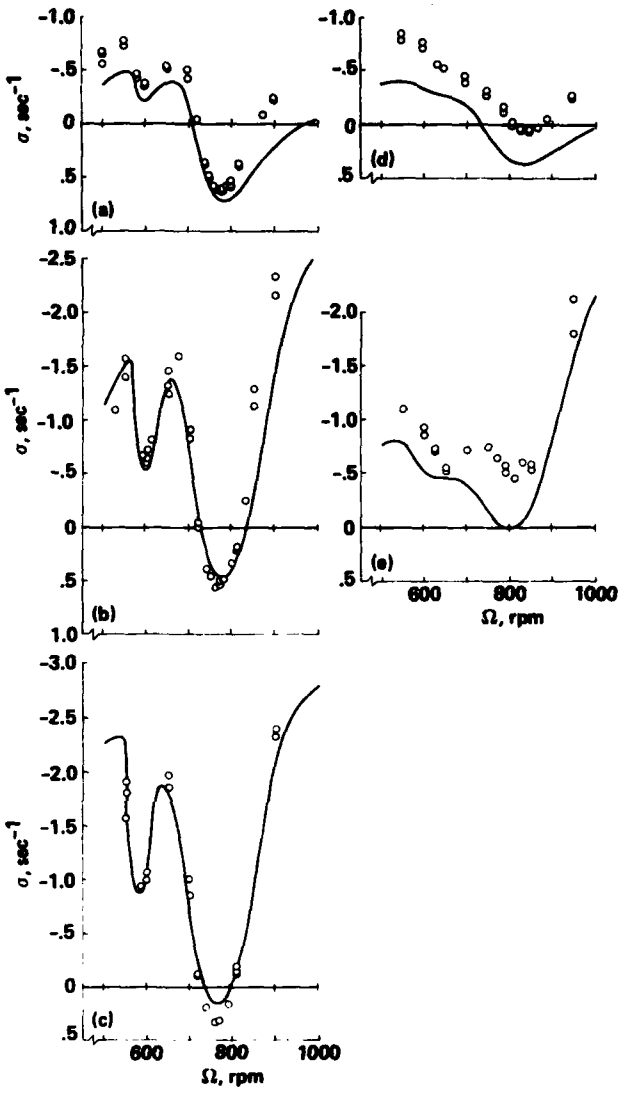

Figure 3. Lead-lag regressing mode damping as a function of rotor speed for $\theta_b = 9°$.

(a) Configuration 1; $\omega_{\beta o} < \omega_{\zeta o}$, $\theta_\zeta = 0$.

(b) Configuration 2; $\omega_{\beta o} < \omega_{\zeta o}$, $\theta_\zeta = -0.4$.

(c) Configuration 3; $\omega_{\beta o} < \omega_{\zeta o}$, $\theta_\zeta = -0.4$, structural flap lag coupling.

(d) Configuration 4; $\omega_{\beta o} = \omega_{\zeta o}$, $\theta_\zeta = 0$.

(e) Configuration 5; $\omega_{\beta o} = \omega_{\zeta o}$, $\theta_\zeta = -.0.4$.

body roll modes – a classical type of air resonance instability. The agreement of the theory and experiment is quite good until the damping starts to recover beyond the most unstable point. Here, the theory fails to predict the extent of the recovery measured by the experiment.

When negative pitch-lag coupling is added to the baseline case, as shown in Figure 3(b) for Configuration 2, the damping is increased over the full range of rotor speeds. This effect is most pronounced when the lead-lag regressing mode is separated from the pitch and roll modes. Although the damping has been increased at the unstable condition, the lead-lag regressing mode is still unstable. The agreement between the experiment and the theory of Reference 3 is quite good in this case, although the recovery in damping for rotor speeds beyond the instability is again greater in the experimental case than that predicted by theory. These results may also be compared qualitatively with Reference 1 where it was predicted that pitch-lag coupling would stabilize the lead-lag regressing mode in the vicinity of the body roll mode, and destabilize it in the vicinity of the body pitch mode, in essence reversing the body mode that couples with the rotor to cause the instability. Similar trends are seen in the experimental results. From 550 to 650 rpm, the body pitch mode has a strong destabilizing effect on the lead-lag regressing mode, although the rotor does remain stable. The lead-lag regressing mode damping is increased in the vicinity of the body roll mode, but is still unstable. That the experimental measurements do not show better correspondence with the predictions of Reference 1 suggests that the results are sensitive to some of the configuration parameters that could not be matched between the experiment and theory.

The combination of negative pitch-lag coupling and structural flap-lag coupling has effects similar to the case of pitch-lag coupling alone. The damping for Configuration 3, as shown in Figure 3(c), is increased over the Configuration 2 results. However, the lead-lag regressing mode still becomes unstable where it encounters the body roll mode. The correlation between the data and the theory of Reference 3 is quite good, although the instability is somewhat stronger than predicted by theory. The analysis of Reference 1 has predicted that this configuration should be completely stable. That it is not, again suggests that the coupling of the lead-lag regressing mode and the body modes is sensitive to configuration parameters.

The results for the matched stiffness configurations show a number of differences from the configurations with conventional stiffness. The damping for Configuration 4, which is matched stiffness without pitch-lag or flap-lag coupling, shows a much shallower unstable region than for the equivalent Configuration 1 case [cf. Figs. 3(d) and 3(a)]. The experimental measurements show only a slight amount of instability, but the correlation in this case is not as good as the previous cases, and the theory shows a considerably larger

region of instability. The reason for this disagreement is not known but appears to be related to the amount of blade pitch angle. It will be discussed further below.

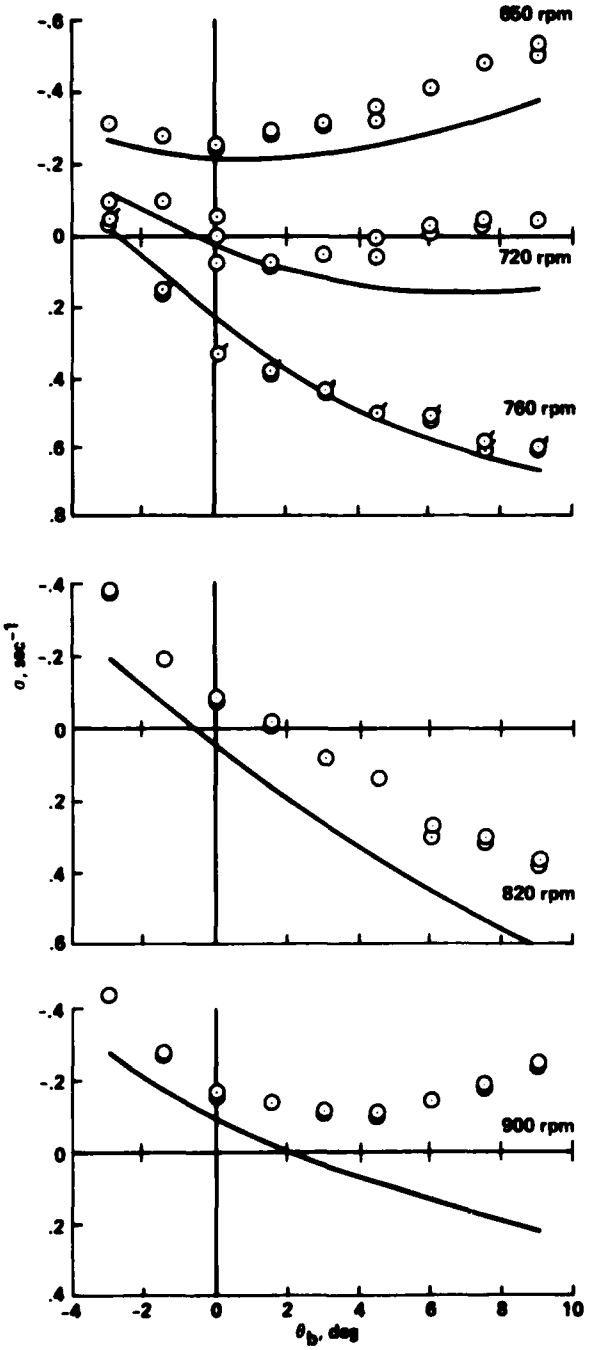

Figure 4. Lead-lag regressing mode damping as a function of blade pitch angle for Configuration 1; $\omega_{\beta o} < \omega_{\zeta o}$, $\theta_\zeta = 0$.

When negative pitch-lag coupling and matched stiffness are combined, as in Configuration 5, the lead-lag regressing mode is stabilized and no instability occurs, as shown in Figure 3(e). For this case the experimental data show that the damping is reduced in the vicinity of both body pitch and roll modes, but the rotor is stable in each case. Disagreement with the theory is again seen with the theory showing less damping, as for Configuration 4. This difference is greatest for the 9° pitch-angle case, and is not seen at a pitch angle of zero. These results are also in qualitative agreement with Reference 1, which predicts that negative pitch-lag coupling will stabilize the air resonance mode for a matched stiffness configuration. Although not shown here, the ground resonance condition with zero blade pitch angle was unstable.

The correlation shown in Figure 3 gives confidence in the adequacy of the theoretical model at a blade pitch angle of 9°. However, it is also of interest to compare the theory and experiment over a range of pitch angles. Figure 4 shows the lead-lag regressing mode damping as a function of pitch angle for Configuration 1. Here the damping is plotted for five rotor speeds, and pitch angles ranging from -3 to +9°. In most cases, the theoretical prediction is somewhat lower than the measured values, but in general there is good agreement between theory and experiment. An exception is the case of Ω = 900 rpm, where the difference between theory and experiment becomes progressively greater for pitch angles above +3°.

The damping as a function of pitch angle for Configuration 3 is shown in Figure 5 for five rotor speeds. These results are representative of both Configurations 2 and 3. The correlation here is generally quite good, except in the area of neutral stability where the data appear somewhat ill-behaved. It was noted during the experiment for these configurations that the damping was dependent upon the amplitude of the excitation for cases near neutral stability, although for the 5 sec record length that was analyzed, there was no obvious nonlinearity in the moving-block function.

The disagreement between theory and experiment that is seen in Figure 3(d) for Configuration 4 is more readily understood by examining the behavior of the lead-lag damping as a function of pitch angle as shown in Figure 6. In this figure, we see a behavior that is consistent at all rotor speeds. At -3 or 0°, the experiment and theory agree very well (see also Fig. 10(b)). As pitch angle increases, there is a progressively increasing deviation, with the experiment showing higher values of damping

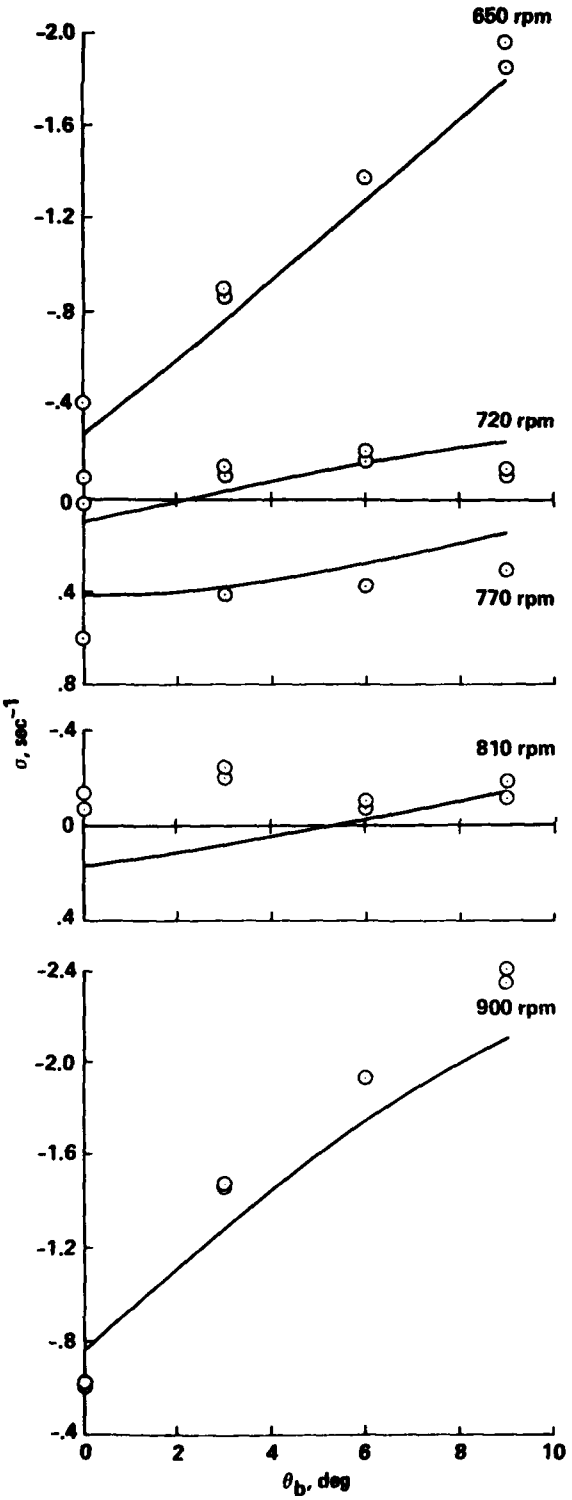

Figure 5. Lead-lag regressing mode damping as a function of blade pitch angle for Configuration 3; $\omega_{\beta o} < \omega_{\zeta o}$, $\theta_\zeta = -0.4$, structural flap-lag coupling.

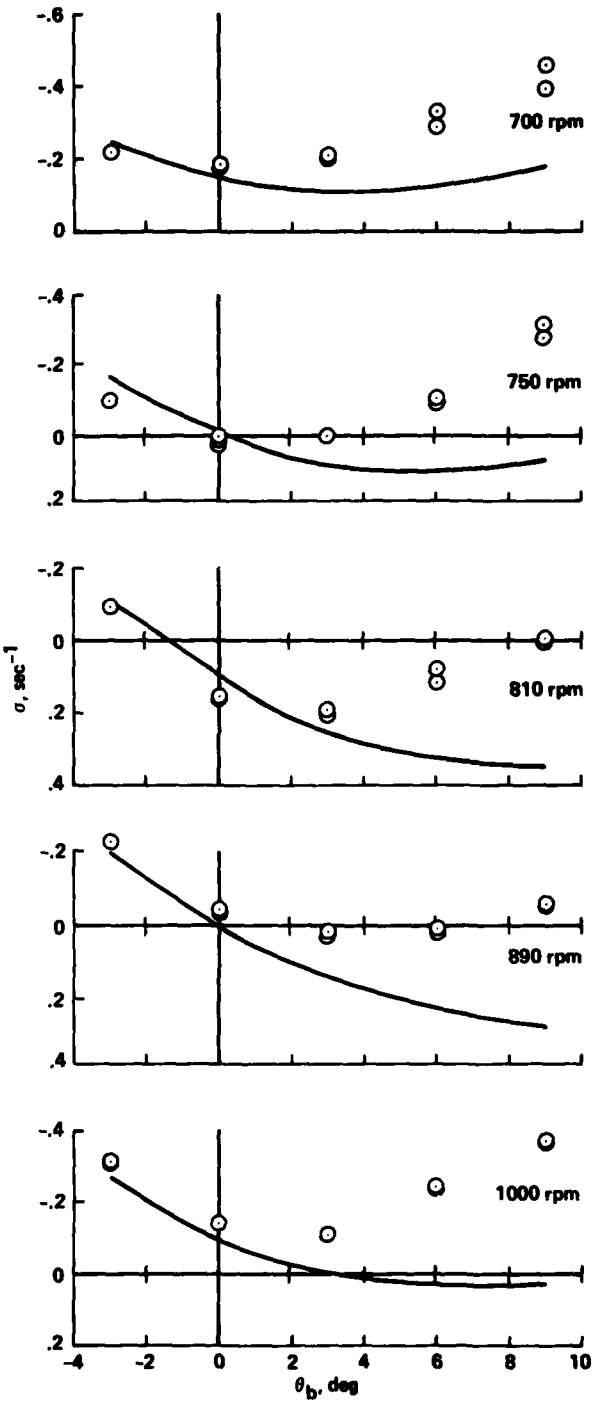

Figure 6. Lead-lag regressing mode damping as a function of blade pitch angle for Configuration 4; $\omega_{\beta o} = \omega_{\zeta o}$, $\theta_\zeta = 0$.

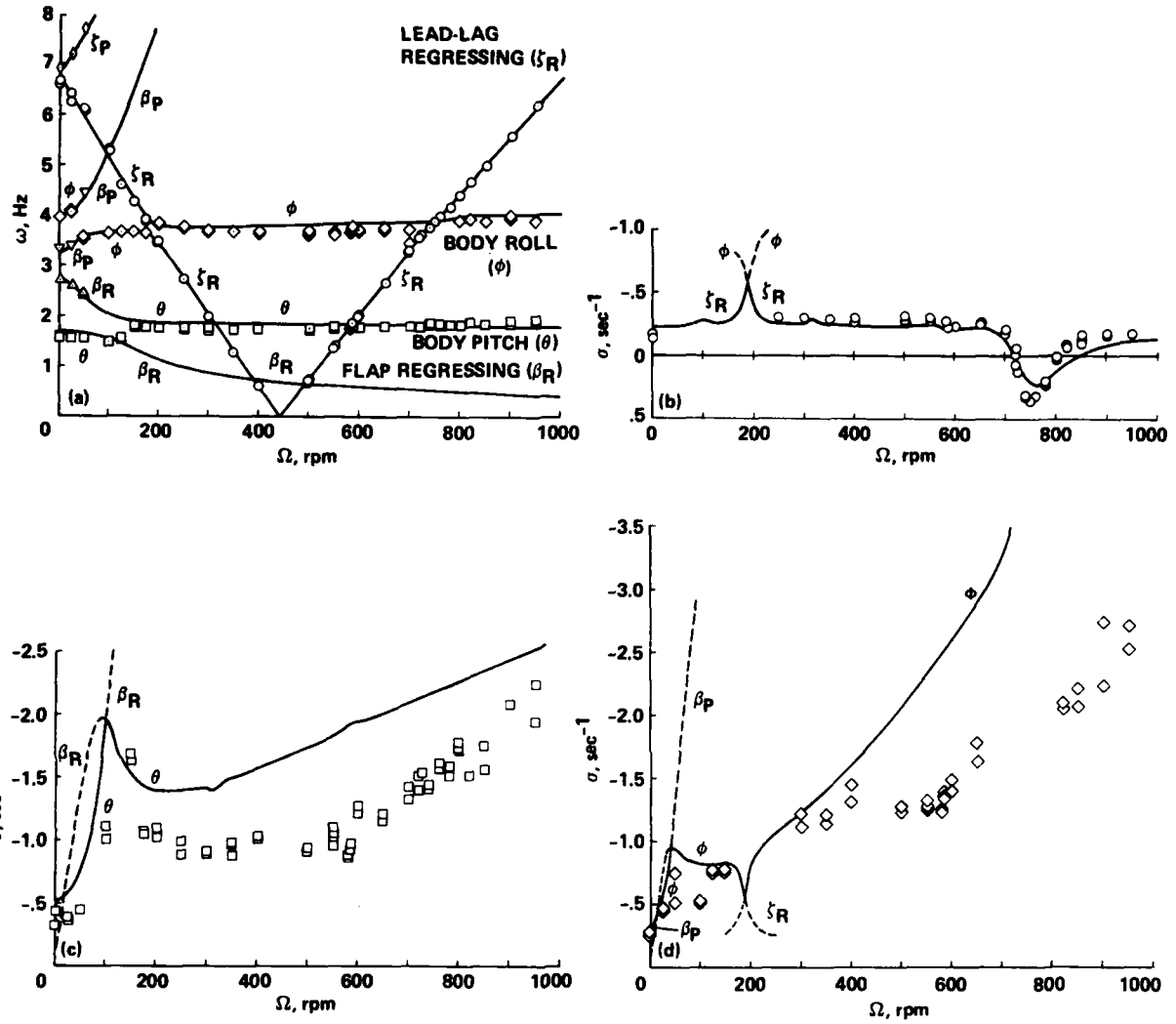

Figure 7. Modal frequency and damping as a function of rotor speed for Configuration 1; $\omega_{\beta o} < \omega_{\zeta o}$, $\theta_\zeta = 0$, $\theta_b = 0°$.

(a) Modal frequencies.

(b) Lead-lag regressing mode damping.

(c) Body pitch mode damping.

(d) Body roll mode damping.

than the theory. The reason for this systematic difference is not known, but it is interesting to speculate that it is due to the nonlinear lift and drag characteristics of the airfoil that are so noticeable at low Reynolds number. It was shown in Reference 8 that these nonlinear airfoil characteristics can have a significant effect on the lead-lag damping of an isolated blade, and that the change in damping is not intuitive. For instance, while the higher profile drag coefficient at an increased pitch angle will increase damping, the slope of the drag curve can cause a decrease in damping. In addition, the extent of these effects also depends on the blade configuration, such as lead-lag frequency and the amount of flap-lag coupling. Whether this is indeed the explanation for the differences seen in Figure 6 cannot be answered with the present theoretical model.

Body Mode Frequency and Damping

The lead-lag regressing mode is the critical mode in the design of a soft inplane hingeless rotor, as this is the mode that will become unstable under air or ground resonance conditions. However, the

other modes are important when a more complete understanding of coupled rotor-body stability is desired. This is especially true in comparing theory and experiment, and in assessing any limitations of the theoretical model. For Configurations 1 and 4, the range of rotor speeds tested was extended to include values from 0 to 1000 rpm. The damping and frequency of all the modes were tracked at the zero pitch-angle condition, and these results are shown in Figure 7 for Configuration 1. The frequencies for all modes are shown in Figure 7(a), and the symbols represent the respective modes as determined experimentally. In most cases, the modes were identified by the coordinate they predominated in, that is, the lead-lag regressing mode in the lead-lag sine or cosine coordinate, body pitch mode in the body pitch coordinate, and so forth. In cases of strong coupling between modes, it was sometimes necessary to identify the mode by its mode shape, that is, the relative amplitude and phase of the modal response in the six coordinates used for analysis. The modal damping measurements are compared with theory in Figures 7(b), 7(c), and 7(d) for the lead-lag regressing, body pitch, and body roll modes, respectively. At the lowest rotor speeds there is strong coupling between the body and rotor flapping modes. The frequency measurements show good agreement in this region, although as rotor speed increases the flap regressing and progressing mode damping increase so quickly that their modal frequencies can no longer be estimated from transient excitation. The body modal damping agreement in this region is only fair. At about 200 rpm, the lead-lag regressing and body roll modes become strongly coupled. The theory and experiment show good agreement for the frequencies, but due to the proximity of the modes, suitable estimates of the damping could not be obtained with the moving-block analysis.

Beyond 250 rpm, the various modes have sorted themselves out, and a consistent trend becomes apparent in the body modal damping. The measured damping is significantly lower than the theoretical prediction, about 40% for both the body pitch and roll modes. Structural damping contributes about 10 or 20% of the body damping; the rest is due to rotor aerodynamics, which suggests that the deficiency in damping is aerodynamic in origin. In Reference 9 it is shown that inflow dynamics have a very strong effect on the damping of the flap regressing mode of a system restricted to rotor flapping and inflow degrees of freedom. In this reference it is shown that the damping is essentially zero with no inflow, and as blade pitch is increased there is a recovery in damping, although it never reaches the level that is predicted by a model that does not include inflow degrees of freedom. The flap progressing mode, which is at a much higher frequency, is not affected by changes in pitch angle. Although similar calculations have not been reported for systems with body degrees of freedom, it is suggested that much of the difference that is seen here for this low inflow condition is due to dynamic inflow.

If in fact dynamic inflow is the reason for the difference between the theoretically predicted body modal damping and the experimental measurements, then as blade pitch angle increases, the damping should partially recover to the predicted level. This hypothesis is examined in Figures 8 and 9, where the body pitch and roll mode damping are shown as a function of pitch angle at a rotor speed of 650 rpm. The body pitch mode damping shows a deficiency in damping at low pitch angle that appears to recover fully by a pitch angle of 4°, and within the scatter of the data is symmetric about the zero inflow condition. But the body roll damping results show a different trend. As seen in Figure 9, the damping deficiency at zero blade pitch angle stays the same over all pitch angles. These two very different results cannot be easily reconciled with intuitive notions of the effect of dynamic inflow. Resolution of this question must await calculations with dynamic inflow included, or perhaps an approximation using a reduced Lock number formulation.[9]

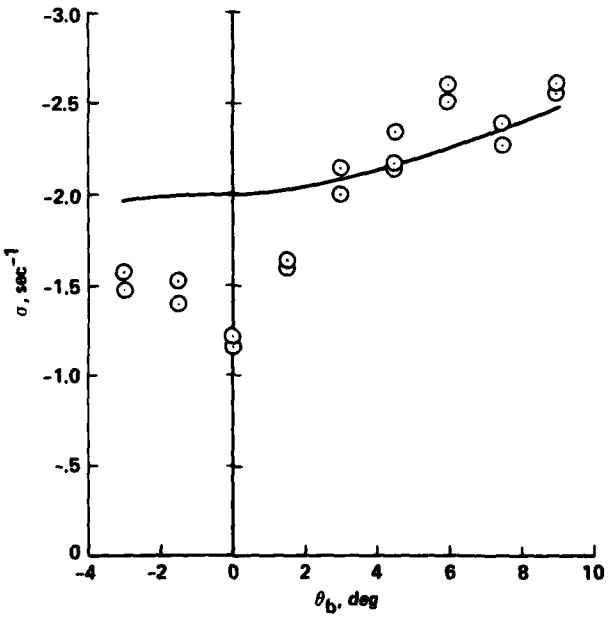

Figure 8. Body pitch mode damping as a function of blade pitch angle for Configuration 1; $\omega_{\beta_o} < \omega_{\zeta_o}$, $\theta_\zeta = 0$, $\Omega = 650$ rpm.

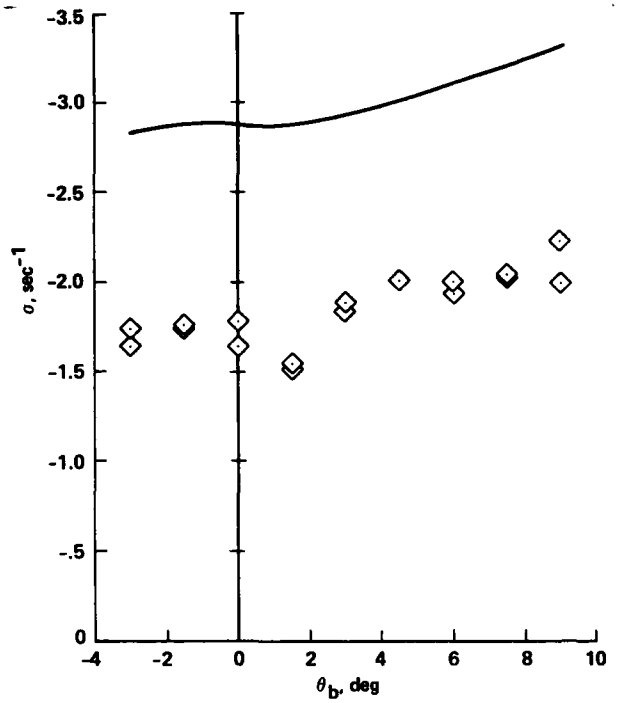

Figure 9. Body roll mode damping as a function of blade pitch angle for Configuration 1; $\omega_{\beta o} < \omega_{\zeta o}$, $\theta_\zeta = 0$, $\Omega = 650$ rpm.

Body modal damping measurements were also made for Configurations 2 and 3 for rotor speeds from 500 to 1000 rpm. The reduction in damping at zero blade pitch, the recovery in damping for the body pitch mode, and the lack of recovery for the body roll mode that are seen for these configurations are essentially identical to the results shown here for Configuration 1.

It has not been demonstated here that the difference between theory and experiment for the body modal damping is due to dynamic inflow, although this is considered the most likely explanation. That no comparable effect is seen in the lead-lag regressing mode suggests that lead-lag regressing-mode damping may be adequately calculated using conventional analyses that do not include dynamic inflow.

The modal frequencies and damping of Configuration 4 were also followed over a rotor speed range of 0 to 1000 rpm. The results are shown in Figure 10, and although the only difference in this configuration from the previous one is an increase in the flap flexure thickness to provide a matched stiffness condition, the modal frequencies and damping show considerable differences. At zero rotor speed, the flap progressing and regressing, and lead-lag progressing and regressing mode frequencies are in close proximity due to the matched stiffness condition. As rotor speed is increased, the progressing and regressing modes rapidly separate. The theory predicts that the flap regressing and body roll modes are strongly coupled, and at rotor speeds beyond 300 rpm switch character. The experimental results indicate that the coupled behavior is quite different, the modal frequencies appear to come much closer before switching modes, and the level of damping where the modes switch is lower than the prediction. As rotor speed is further increased, the theory predicts that the flap regressing mode damping becomes quite large and the mode does not couple with the body pitch mode. However, in the experimental case, measurements in the pitch coordinate show two modes of comparable damping at rotor speeds beyond 350 rpm, one mode at about 0.8 Hz and the other at about 2.0 Hz. These two modes are very similar in mode shape with approximately equal amounts of pitching, rolling, and flapping motion. Slight differences are observed in the mode-shape phase, with the lower-frequency mode having pitching and rolling motions in quadrature, while the higher-frequency mode has the pitching and rolling motions in phase. To call one mode the body pitch mode, and the other the flap regressing mode is somewhat arbitrary; the rationale used here is that as blade pitch angle increases only one of these modes remains, and it is assumed to be the body pitch mode.

Beyond 300 rpm, the body roll mode damping in Figure 10(d) shows behavior quite similar to Configuration 1. However, both the theoretical and measured damping levels are considerably higher than in the previous case. The behavior of the body pitch mode is very different than before because of the presence of the two modes. The theoretical prediction is of little value in interpreting these results, and the experimental data scatter is sufficient to inhibit any but the most optimistic guesses. Nevertheless, it is suggested that the data bear evidence of two modes that cross at approximately 500 rpm creating a cusp. The character of the mode with the lower damping is in all cases the body pitch mode, and it is proposed that beyond the hypothetical cusp, the flap regressing mode shows the higher damping.

The data given for Configuration 1 in Figure 7 showed very good agreement with theory, with the exception of the body mode damping. While the only difference in the present configuration is an eightfold increase in flapping stiffness, this has had a significant impact on the measured system behavior, and the correlation is substantially degraded. There is strong evidence that the flap regressing mode

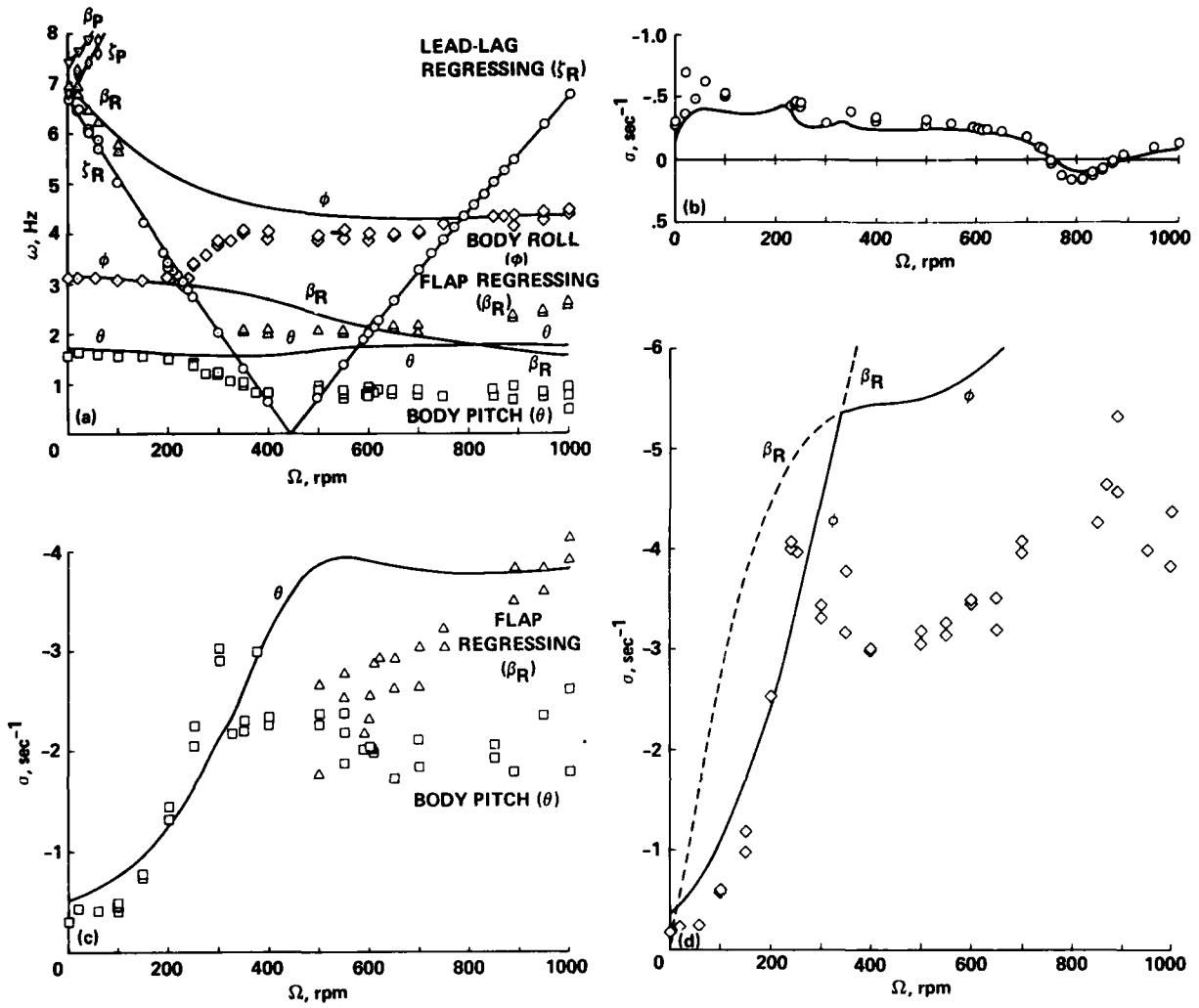

Figure 10. Modal frequency and damping as a function of rotor speed for Configuration 4; $\omega_{\beta o} = \omega_{\zeta o}$, $\theta_\zeta = 0$, $\theta_b = 0°$.

(a) Modal frequencies.

(b) Lead-lag regressing mode damping.

(c) Body pitch and flap regressing mode damping.

(d) Body roll mode damping.

which theory predicts would be very heavily damped and undetectable in the experimental measurements, is in fact relatively lightly damped for this low inflow condition, and strongly coupled with the body pitch mode. The very limited body mode data that were taken at blade pitch angles above zero show only a single mode in the pitch coordinate, and the inference is that the flap regressing mode damping increases so as to be undetectable in the measurements. It seems likely that at least some of the behavior seen here is related to dynamic inflow. However, why the strong coupling of the body pitch and flap regressing modes that is seen here was not detected in Configuration 1 is not understood.

Conclusion

The aeromechanical stability of five rotor configurations was investigated at model scale, and information about modal frequencies and damping was obtained. The experimental results were compared with theory, and the following conclusions drawn.

1. For the nonmatched stiffness configuration, the addition of negative pitch-lag coupling stabilized the lead-lag regressing mode when compared to the baseline case. There was a substantial increase in damping away from the air-resonance mode instability, but the modal damping was improved only slightly in the area of the instability.

2. For the nonmatched stiffness configuration, the combined effect of negative pitch-lag and structural flap-lag coupling provided some additional damping over the case of negative pitch-lag coupling alone. The lead-lag regressing mode still became unstable under air resonance conditions.

3. The matched stiffness configuration showed a region of instability substantially less severe than for the baseline configuration. The lead-lag regressing-mode damping in this case showed a shallower aspect than the baseline.

4. The addition of negative pitch-lag coupling to the matched stiffness configuration was stabilizing, and the air resonance instability was eliminated.

5. The correlation between the experimental results and theoretical model of Reference 3 was, in general, very good for the lead-lag regressing mode for the nonmatched stiffness configurations. For the matched stiffness configurations, there was a systematic difference between experiment and theory for blade pitch angles greater than 3°.

6. Modal frequency and damping were examined for rotor speeds from 0 to 1000 rpm for the baseline configuration. At zero blade pitch angle, correlation was in general very good, except the body modal damping predicted by theory was significantly higher than the measurements. It was suggested that the deficiency in damping was due to the inflow dynamics, and that this effect would be reduced as blade pitch angle and the steady inflow increased. This did occur for the body pitch mode damping, but not for the body roll mode.

7. Modal frequency and damping for the matched stiffness configuration exhibited more complex behavior than seen for the baseline case. Correlation of theory and experiment for the body modes was poor, and it was suggested that this was due to the effect dynamic inflow had on the damping of the flap regressing mode.

8. Whether differences seen in body modal damping and behavior are due to the inflow dynamics, or some other cause, accurate calculation of the lead-lag regressing mode frequency and damping appears feasible with present analyses.

References

1. Ormiston, Robert A. "Aeromechanical Stability of Soft Inplane Hingeless Rotor Helicopters." Paper No. 25, Third European Rotorcraft and Powered Lift Aircraft Forum, Aix-en-Provence, France, Sept. 1977.

2. Bousman, William G., and Hodges, Dewey H. "An Experimental Study of Coupled Rotor-Body Aeromechanical Instability of Hingeless Rotors in Hover." Vertica, 3, Dec. 1979, pp. 221-244.

3. Hodges, Dewey H. "A Theoretical Technique for Analyzing Aeroelastic Stability of Bearingless Rotors." Proceedings of the 19th AIAA/ASME Structures, Structural Dynamics and Material Conference, April 1978, pp. 282-294.

4. Donham, R. E., Cardinale, S. V., and Sachs, I. B. "Ground and Air Resonance Characteristics of a Soft In-plane Rigid-Rotor System." Journal of the American Helicopter Society, 14, no. 4, Oct. 1969, pp. 33-41.

5. Lytwyn, R. T., Miao, W., and Woitsch, W. "Airborne and Ground Resonance of Hingeless Rotors." Journal of the American Helicopter Society, 16, no. 2, April 1971, pp. 2-9.

6. Miao, Wen-liu, Edwards, W. Thomas, and Brandt, David E. "Investigation of Aeroelastic Stability Phenomena of the Helicopter by In-flight Shake Test." NASA Symposium on Flutter Testing Techniques, NASA SP-415, Oct. 1975, pp. 473-499.

7. Staley, James A., Gabel, Richard, and MacDonald, H. I. "Full Scale Ground and Air Resonance Testing of the Army-Boeing Vertol Bearingless Main Rotor." Preprint No. 79-23, American Helicopter Society 35th Annual Forum Proceedings, May 1979.

8. Ormiston, R. A., and Bousman, W. G. "A Study of Stall-Induced Flap-Lag Instability of Hingeless Rotors." Preprint No. 730, American Helicopter Society 29th Annual Forum Proceedings, May 1973.

9. Ormiston, Robert A. "Application of Simplified Inflow Models to Rotorcraft Dynamic Analysis." Journal of the American Helicopter Society, 21, no. 3, July 1976, pp. 34-37.

Appendix

Geometric and descriptive properties are given in Table 2. The Lock number is calculated assuming a value of the lift curve slope of 5.73, and using the flapping inertia of the blade about the flexure center from Table 3. The lift coefficient of the NACA 23012 airfoil at zero angle of attack is 0.15. The profile drag coefficient is derived from steady-bending moment data.

Blade mass properties are given in Table 3. The blade mass, centroid, and flap inertia were determined from the mean of three blades. The polar inertia was derived from design drawings and the blade flap inertia.

Blade frequency and damping were obtained from measurements on individual blades. These values are tabulated by configuration in Table 4. The blade/flexure structural damping η_ζ is expressed as a percent of critical damping.

The body mass properties were determined by weighing individual components. The gimbal frame acts as a portion of the body during pitch motions, but not during roll motions. Thus, weight and vertical c.g. values are given with respect to pitch or roll axes. The body mass properties are shown in Table 5. The vertical c.g. is above the gimbal pivot plane. The model was ballasted in pitch and roll to place the longitudinal and lateral c.g.'s at the gimbal pivot point. The distance from gimbal plane to the rotor disk is 24.1 cm. Body inertias were calculated from measurements of body-spring stiffnesses and body frequencies, assuming the body acted as a single degree-of-freedom oscillator. The body pitch and roll mode damping in terms of percent critical is:

$$\eta_\theta = 3.20\%$$

$$\eta_\phi = 0.929\%$$

Table 2. Rotor Geometric and Descriptive Properties

Property	Value
Radius, cm	81.1
Chord, cm	4.19
Hinge offset, cm	8.51
Lock number	7.37
Blade profile	NACA 23012
Profile drag coefficient	0.0079

Table 3. Blade Mass Properties

Property	Value
Blade mass, (to flap flexure centerline), g	209
Blade mass centroid (ref. flexure centerline), cm	18.6
Blade flap inertia (ref. flexure centerline), g-m^2	17.3
Blade polar inertia (ref. hub centerline), g-m^2	85.5

Table 4. Blade Frequency and Damping

Configuration	$\omega_{\beta o}$, Hz	$\omega_{\zeta o}$, Hz	η_ζ, %
1	3.13	6.70	0.52
2	3.13	7.16	0.65
3	3.13	7.16	0.65
4	6.63	6.73	0.53
5	6.64	7.04	0.65

Table 5. Body Mass Properties

Property	Pitch	Roll
Body mass, kg	22.60	19.06
Vertical c.g., cm	1.32	1.56
Body inertia, g-m^2	633	183